Quantifying the Sensitivity of Target Dose on Intrafraction Displacement in Intracranial Stereotactic Radiosurgery

Practical Radiation Oncology® (2022) 12, e221–e231

practical radiation oncology
pro
www.practicalradonc.org

Original Report

Quantifying the Sensitivity of Target Dose on Intrafraction Displacement in Intracranial Stereotactic Radiosurgery

Jannie Schasfoort, MSc,[a,*] Mark Ruschin, PhD,[b] Arjun Sahgal, MD,[b] R. Lee MacDonald, PhD,[b] Young Lee, PhD,[b] Carola van Pul, PhD,[c] Patrick Langenhuizen, PhD,[d] Patrick Hanssens, MD,[e,f] Guus Beute, MD,[e] Frits Wittkamper, PhD,[g] and Jan-Jakob Sonke, PhD[g]

[a]*Gamma Knife Center Tilburg, Department of Medical Physics, Elisabeth-TweeSteden Hospital, Tilburg, The Netherlands;* [b]*Department of Radiation Oncology, Sunnybrook Health Sciences Centre, University of Toronto, Toronto, Ontario, Canada;* [c]*Department of Applied Physics, Eindhoven University of Technology, Eindhoven, The Netherlands;* [d]*Department of Electrical Engineering, Eindhoven University of Technology, Eindhoven, The Netherlands;* [e]*Gamma Knife Center Tilburg, Department of Neurosurgery, Elisabeth-TweeSteden Hospital, Tilburg, The Netherlands;* [f]*Gamma Knife Center Tilburg, Elisabeth-TweeSteden Hospital, Tilburg, The Netherlands; and* [g]*Department of Radiation Oncology, The Netherlands Cancer Institute, Amsterdam, The Netherlands*

Received 2 September 2021; accepted 30 November 2021

Abstract

Purpose: Mask-immobilized stereotactic radiosurgery (SRS) using a gating window is an emerging technology. However, the amount of intracranial tumor motion that can be tolerated during treatment while satisfying clinical dosimetric goals is unknown. The purpose of this study was to quantify the sensitivity of target dose to tumor motion.

Methods and Materials: In clinical SRS plans, where a nose marker was tracked as surrogate for target motion, translational and rotational target movements were simulated using nose-marker displacements of ±0.5 mm, ±1.0 mm, or ±1.5 mm. The effect on minimum dose to 99% of the target (D_{99}) and percent target coverage by prescription dose was quantified using mixed-effect modeling with variables: displacement, target volume, and location.

Results: The effect on dose metrics is statistically larger for translational displacements compared with rotational displacements, and the effect of pitch rotations is statistically larger compared with yaw rotations. The mixed-effect model for translations showed that displacement and target volume are statistically significant variables, for rotation the variable target distance to rotation axis is additionally

Sources of support: This work had no specific funding.

Disclosures: Dr Ruschin is the coinventor of and owns associated intellectual property specific to the image guidance system on the Gamma Knife Icon. Dr Saghal reports the following: advisor/consultant with Abbvie, Merck, Roche, Varian (Medical Advisory Group), Elekta (Gamma Knife Icon), BrainLAB, and VieCure (Medical Advisory Board); board member of the International Stereotactic Radiosurgery Society (ISRS); past educational seminars with Elekta AB, Accuray Inc, Varian (CNS Teaching Faculty), Brainlab, Medtronic Kyphon; research grant with Elekta AB; travel accommodations/expenses by Elekta, Varian, and BrainLAB. Dr Sahgal also belongs to the Elekta MR Linac Research Consortium and the Elekta Spine, Oligometastases, and Linac-based SRS Consortia. Dr MacDonald has an existing intellectual property license agreement with Brainlab AG for stereotactic radiosurgery dosimetric planning algorithms. Dr Langenhuizen reports nonfinancial support from Elekta AB, grants from ZonMW, grants from Elekta AB, outside the submitted work. Dr Beute reports personal fees from Elekta AB, outside the submitted work, and presidency of the Leksell Gamma Knife Society meeting in 2016. Dr Sonke reports grants from Elekta Oncology Systems AB and License fees from Elekta Oncology Systems AB, outside the submitted work. The remaining authors have nothing to disclose.

Research data are stored in an institutional repository and will be shared upon request to the corresponding author.

* Corresponding author.; E-mail: j.schasfoort@etz.nl

https://doi.org/10.1016/j.prro.2021.11.012

significant. For mean target volume (12.6 cc) and translational nose-marker displacements of 0.5 mm, 1.0 mm, and 1.5 mm, D_{99} decreased by 2.2%, 7.1%, and 13.0%, and coverage by 0.4%, 1.8%, and 4.4%, respectively. For mean target volume, mean distance midpoint-target to pitch axis (7.6cm), and rotational nose-marker displacement of 0.5 mm, 1.0 mm, and 1.5 mm, D_{99} decreased by 1.0%, 3.6%, and 6.9%, and coverage by 0.2%, 0.8%, and 1.9%, respectively. For rotational yaw axis displacement, mean distance midpoint-target axis (4.2cm), D_{99} decreased by 0.3%, 1.2%, and 2.5%, and coverage by 0.1%, 0.2%, and 0.5%, respectively.

Conclusions: Simulated target displacements showed that sensitivity of tumor dose to motion depends on both target volume and target location. Suggesting that patient- and target-specific thresholds may be implemented for optimizing the balance between dosimetric plan accuracy and treatment prolongation caused by out-of-tolerance motion.

Introduction

Historically, stereotactic radiosurgery (SRS) has been delivered in a single fraction with submillimeter accuracy using frame fixation for patient immobilization.[1,2] With the development of image guided SRS, noninvasive mask immobilization is increasingly used for patient comfort, ease in workflow for large volume departments and, moreover, enables multifraction treatments to be delivered more precisely.[2]

A recent development in image guided SRS has been the release of the Gamma Knife Icon (GKI) system (Elekta AB, Stockholm, Sweden). The system integrates a cone beam computed tomography (CBCT) scanner to ensure accurate setup, with a real-time high-definition motion monitoring (HDMM) system to track patient position during treatment, while the patient is immobilized in a GKI-specific thermoplastic mask.[3] The HDMM includes an infrared camera tracking the position of a reflective marker placed on the patient's nose during treatment. When the HDMM is in "active" mode, treatment delivery is either paused or gated automatically, if this nose marker motion exceeds a predefined threshold. If the nose marker remains above the threshold, adjustment of the treatment plan to the new patient position is mandatory and performed by acquiring an intrafraction CBCT. Thus, the system is designed to allow small intrafraction motions during delivery with a user-defined tolerance threshold.

The effect of head immobilization has been investigated by Babic et al and Guckenberger et al. They reported that immobilization using a thermoplastic mask can lead to larger intrafraction motions compared with frame-based rigid immobilization, thereby possibly effecting treatment plan dosimetry.[4,5] In addition, Wright et al showed that for GKI, the displacement of the nose marker is not equal to the displacement of the target.[6] Furthermore Kim et al, Vulpe et al, and MacDonald et al have shown that patients become less tolerant of the thermoplastic mask as treatment time increases.[3,7,8]

Although several studies have reported on the GKI system efficacy concerning (1) technical aspects of the CBCT,[9-11] (2) adaptation of the treatment plan to the new patient position based on the CBCTs,[12-14] and (3) the HDMM tracking system,[4,15] the amount of tumor motion that can be tolerated during treatment while satisfying clinical dosimetric goals is unknown.

The purpose of the present study was to quantify the sensitivity of target dosimetry to tumor motion in a series of GKI-treated patients. Translational and rotational displacements were simulated from actual patient SRS plans, and the effects of displacements were quantified considering tumor volume and location.

Methods

Data collection

Data from the Leksell Gamma Knife Planning system (LGP) were collected for all treatments with mask immobilization between 2016 and 2020 at the Gamma Knife Centrum in Tilburg, Netherlands. Data consisted of RT-DICOM files, LGP header files, and exported dose-volume histogram (DVH). The RT-DICOM data consisted of the magnetic resonance imaging (MRI) data set (slice thickness 1.5 mm), the structure set with delineations and the dose distribution (0.5 mm voxel pitch). The LGP header file contained the geometric transformations between different coordinate systems (Supplementary Materials, Transformations between different coordinate systems) and the prescription dose.

Targets treated multiple times were only included once and neighboring targets closer than 1.5 cm to one another in the same treatment were excluded due to dosimetric crosstalk. Additionally, one patient was excluded based due to abnormal anatomy of the brain, making it impossible to determine landmarks needed for rotation simulation. Patient and treatment characteristics are summarized in Table 1.

The medical ethics committee waived formal approval for this study and the study was approved by the Department of Education and Research, Elisabeth TweeSteden Hospital, Tilburg, Netherlands. All patient data was coded before analyses.

Data was processed and analyzed using MATLAB (Mathworks, version 2014b), including dedicated scripts needed for volume reconstructions and rotational simulations.[16,17] Statistical analyses were performed using R statistics (Rstudio, version 1.2.5033 RStudio, Inc.), including packages "lmer" for the mixed-effect modeling, and "insight"[18] for determining the R-squared of the model.

Table 1 Summary of patient data included in the study

Patient information	Included in study
No. of patients	77
No. of treatments	90
Male/female	35/42
Age (mean, range), y	52.8 (23-83)
Target information	
No. of targets	121
Indication	Meningioma (37)
	NF-2 meningioma (40)
	Metastases (30)
	Plexus papilloma (6)
	Vestibular schwannoma (3)
	ACTH-producing pituitary adenoma (2)
	Nonsecreting pituitary adenoma (1)
	Choroid plexus papilloma (1)
	Hemangiopericytoma (1)
Close to OAR (yes/no)	23/98
Volume <1 cc mean (range), cc	0.39 (0.006-0.983) n = 40
Volume 1-10 cc mean (range), cc	4.1 (1.02-9.97) n = 36
Volume >10 cc mean (range), cc	29.8 (10.2-64.3) n = 45

Abbreviations: ACTH = adrenocorticotropic hormone; NF-2 = Neurofibromatosis type 2; OAR = organ at risk.

Workflow

Every treatment plan was processed and analyzed using the following workflow (Fig 1).

Validation

The DICOM data (ie, images, dose, and contours) were used to generate (1) a triangulated surface, enclosing a 3-dimensional volume representing the target (Fig 1A), and (2) the DVH of the target (Fig 1B). Subsequently, the reconstructed DVH and volume were compared against the calculated DVH and volume from LGP (Fig 1C). If the difference in volume was less than 10%, and the difference in dose to the 99% of the target (D_{99}) was less than 2.5%, the target was included for further analyses.

Simulated translations and rotations

To quantify the effect of tumor motion on the dose distribution, translations (Fig 1D) and rotations (Fig 1E) were simulated for the included targets such that the nose-marker displacement equaled ±0.5 mm, ±1.0 mm, or ±1.5 mm in and around the x-, y-, or z-direction. The x-direction is from left to right, the y-direction from posterior to anterior and the z-direction from inferior to superior.

For translations, a mask of the enclosed 3-dimensional volume was made with a voxel pitch of 0.5 mm. Target translation was simulated by shifting that mask by ±1, ±2, or ±3 voxels in each direction along the MRI-imaging planes, representing a pure 1-dimensional-shift of ±0.5 mm, ±1.0 mm, and ±1.5 mm, respectively.

For rotation simulations, a grid voxel pitch of 0.1 mm was used for making the mask of the 3-dimensional reconstructed volume. Furthermore, the dose distribution was resampled using linear interpolation to the same grid. Rotations were first applied to the voxel coordinates after which a new mask was created on the original grid by rounding these coordinates to the nearest voxel. For its reproducibility across patients, the required rotational axes and origin were defined by 5 anatomic landmarks (Fig 2) from the LGP planning images. These landmarks were identified by the first author (J.S.) and verified by a neurosurgeon (G.B.). The landmarks consisted of the (1) anterior commissure (AC), (2) posterior commissure (PC), (3) midline reference (MR), (4) inferior border of the clivus (ie, the lowest point fixed to the skull), and (5) nose tip. The nose tip is defined by the average position of the nose marker as registered by the HDMM during the acquisition of the setup CBCT. If a shift in AC or PC was caused by the target, their original positions were estimated by a neurosurgeon.

Rotational axes were defined as the normal vectors of 3 perpendicular planes: (1) a sagittal plane formed by AC, PC, and MR, (2) an axial plane with the AC-PC line in plane, perpendicular to the sagittal plane, and (3) a coronal plane perpendicular to both other planes and positioned through the clivus. These 3 planes are not exactly similar to the MRI imaging planes (sagittal, axial, and coronal), because the patients head is not necessarily aligned with the MRI imaging planes. The origin for the rotation was the inferior border of the clivus.

Using these definitions, the y-axis for rotation falls within millimeters of the nose marker (Fig 2). So, to displace the nose marker by 0.5, 1.0, or 1.5 mm large, not representative for a clinical situation, or infeasible rotation angles are needed. Therefore, rotations around the y-axis were not performed.

Rotation around the x-axis corresponds to pitch ("nodding"), and around the z-axis to yaw ("looking left-right"). Due to the definition of rotation axes, the coordinate system for rotation and for translation cannot be precisely equal.

Evaluation metrics

For all simulated translations and rotations, the reconstructed DVH after a displacement (Fig 1F-G) was compared with the original DVH (before displacement, Fig 1B) using the following 2 metrics: (1) D_{99} and (2)

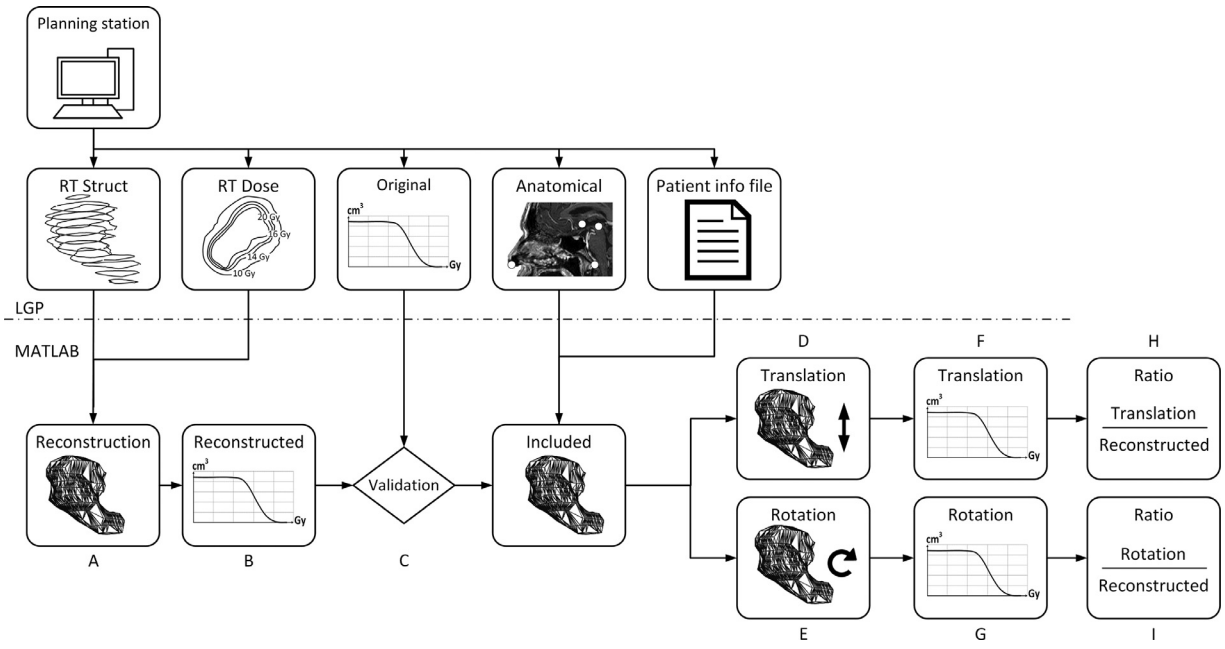

Figure 1 Schematic overview of data processing: reconstruct original (A) volume and (B) dose-volume histogram (DVH) using information from radiation therapy structure (RT-Struct) and dose (RT-Dose), (C) validating volume and DVH against Leksell Gamma Knife Planning system values, only including targets meeting the inclusion criteria, (D) translation, and (E) rotation of volume using the anatomic landmarks and Leksell Gamma Knife Planning system patient-info-file, calculate DVH after (F) translation or (G) rotation, calculating ratio_{D99} and $\text{ratio}_{coverage}$ before and after (H) translation, and (I) rotation.

percent volume of the target receiving the prescribed dose (coverage). The ratio postdisplacement to nominal of D_{99} and coverage was measured and reported as ratio_{D99} and $\text{ratio}_{coverage}$, respectively.

Tumor distance to rotation axis

A dose-calculation box around each target is used for dose calculations in LGP. This box is automatically centered around the target and the midpoint is listed. This midpoint is considered to be a surrogate of the tumor's position with respect to the rotation axes. For translations, the tumor position does not influence the ratio_{D99} or $\text{ratio}_{coverage}$. For rotations, the effect on target dose metrics depends on the relative location of each target to the rotation axis. For each target, 3 metrics were calculated: (1) rotation angle needed to simulate a displacement of ± 0.5, ± 1.0, or ± 1.5 mm of the nose marker based on distance of nose marker to rotation axis, (2) distance of target-box-midpoint to rotation axis (*dist*), and (3) displacement of target-box-midpoint caused by rotation.

Statistical analysis

Ratio_{D99} and $\text{ratio}_{coverage}$ were determined for all simulation-translated and -rotated targets. For ratio_{D99} and $\text{ratio}_{coverage}$, the Wilcoxson signed-rank test was used to statistically compare: (1) displacement versus no displacement, (2) positive versus negative displacements (along each principal axis) to determine whether directionality played a significant role ($P < .05$), (3) displacements along the 3 different axes to determine whether the results depended on the direction of translation or rotation, and (4) translations and rotations to determine whether translations had a different effect than rotations.

For translations, a mixed-effect model was used to evaluate the effect of the fixed effects: (1) nose-marker displacement (*displ*) caused by translation along the axis, (2) target volume (V_{target}), and (3) interaction of *displ* and V_{target} on ratio_{D99} or $\text{ratio}_{coverage}$, Equation 1.

$$outcome = intercept + \alpha_0 * \Delta V + \alpha_1 * displ + \alpha_2 * \Delta V * displ \quad (1)$$

where $\Delta V = V_{target} - V_{mean}$.

For rotations, a mixed-effect model was used to evaluate the effect of the fixed effects: (1) *displ* of the nose marker caused by rotation around an axis, (2) target volume (V_{target}), (3) distance of the target to the rotation axis (*dist*), and (4) interactions between *displ*, and/or

$$outcome = intercept + \beta_0 * \Delta V + \beta_1 * displ + \beta_2 * \Delta dist + \beta_3 * \Delta V * displ + \beta_4 * \Delta V * \Delta dist + \beta_5 * displ * \Delta dist + \beta_6 * \Delta V * displ * \Delta dist \quad (2)$$

V_{target}, and/or *dist* on $ratio_{D99}$ or $ratio_{coverage}$, Equation 2. where $\Delta V = V_{target} - V_{mean}$ and $\Delta dist = dist_{target} - dist_{mean}$.

The models considered the random effects caused by the fact that outcomes belong to a certain target and axis. Displacement needed to be treated as a factor, not as a continuous variable, due to the limited number of simulated displacements of the nose marker (target). Therefore, the model has coefficients for each displacement (*displ*), and $displ = 0$ for no displacement and $displ = 1$ if there is a displacement. The models are described in detail in Supplementary Materials, Mixed-effect models.

Results

$Ratio_{D99}$ and $Ratio_{coverage}$

After extracting all relevant treatments, 157 targets were obtained. Of these, 36 (23%) were excluded using the following criteria: (1) 7 (19.4%) treated multiple times, (2) 9 (25.0%) dosimetric cross-talk, (3) 3 (8.3%) reconstructed volume difference larger than 10%, (4) 16 (44.4%) D_{99} difference larger than 2.5%, and (5) 1 (2.8%) patient was excluded due to abnormal anatomy of the brain.

For all included targets, Figures 3 and 4 illustrate the results for translations and rotations respectively. The target volumes were divided into 3 categories: "<1 cc," "1 to 10 cc," and ">10 cc."

To obtain a ±0.5 mm displacement of the nose marker caused by rotation, the rotation angle required was mean (range) 0.25 (0.21-0.29) degrees. For the ±1.0 mm and ±1.5 mm nose-marker displacements the rotation angle increased linearly. For all displacements the effect on D_{99} and coverage was statistically different compared with no displacement ($P < .001$).

For all targets, no statistically significant difference ($P > .05$) in either $ratio_{D99}$ and $ratio_{coverage}$ between positive and negative translations or rotations was found (Table E1a).

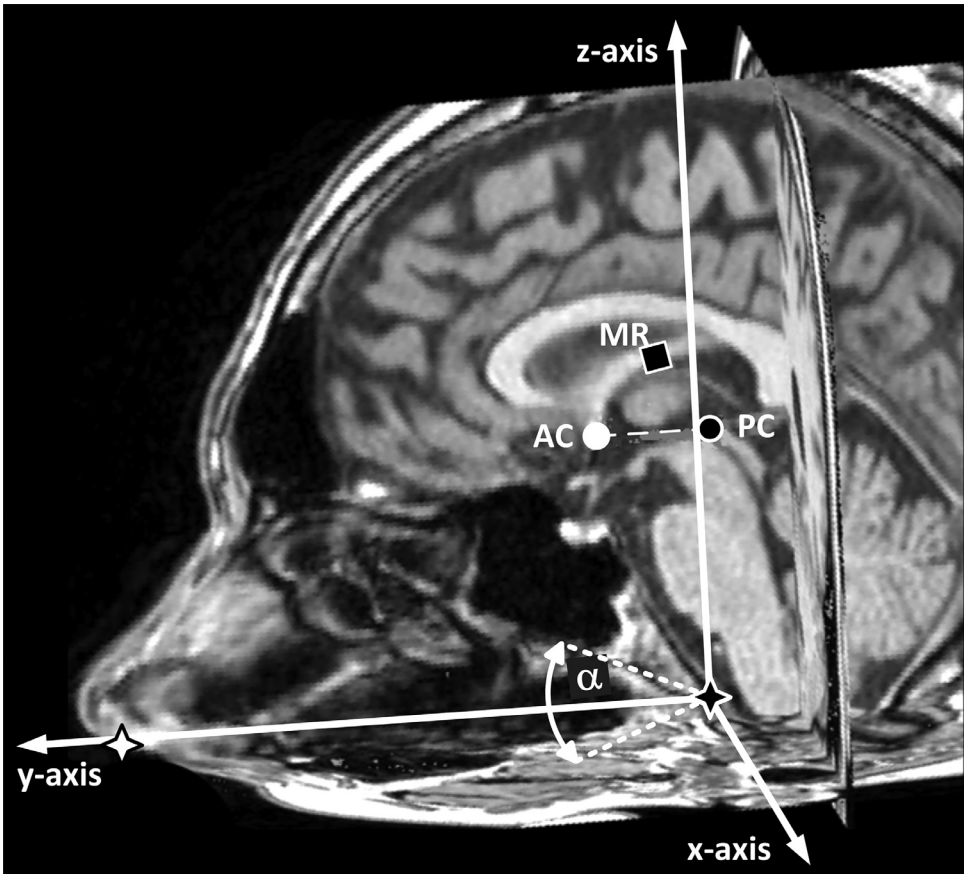

Figure 2 Anatomic landmarks to define rotational axes. The solid dot is the anterior commissure (AC), the open dot is the posterior commissure (PC), open square is midline reference (MR), the black star is inferior border of the clivus, and white star shows position of the nose marker. The angle α was calculated so that nose-marker displacement equaled ±0.5 mm, ±1.0 mm, or ±1.5 mm.

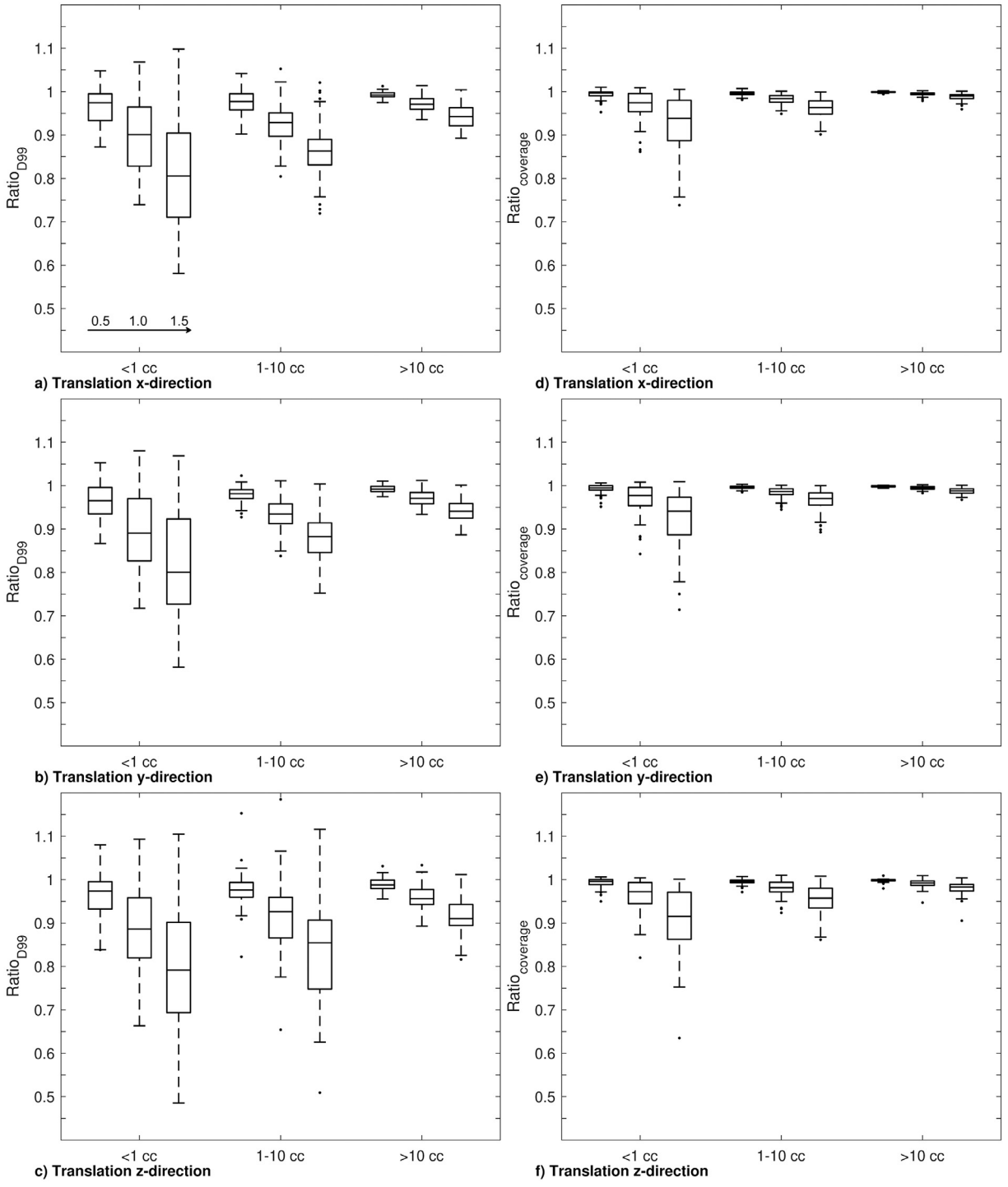

Figure 3 Boxplots of ratio$_{D99}$ (left) and ratio$_{coverage}$ (right) per volume category, subdivided in translation directions in x-direction (a, c), y-direction (b, d), and z-direction (c, e). Per volume category displacement increased from 0.5 mm to 1.5 mm from left-to-right.

Therefore, the averaged outcomes from the positive and negative displacements were used for the mixed-effect model.

The dosimetric effect of translational displacements along the different axes were significantly different for x- versus z-direction, and y- versus z-direction for nose displacements ≥1.0 mm, for both ratio$_{D99}$ and ratio$_{coverage}$. Rotational displacements around the x-axis were significantly larger than those around the z-axis ($P < .01$). The resulting P values are listed in Table E1b. The mixed-effect model for translation was fitted as a single model for all directions combined, and for rotation separate models were fitted for each rotational axis. The statistical

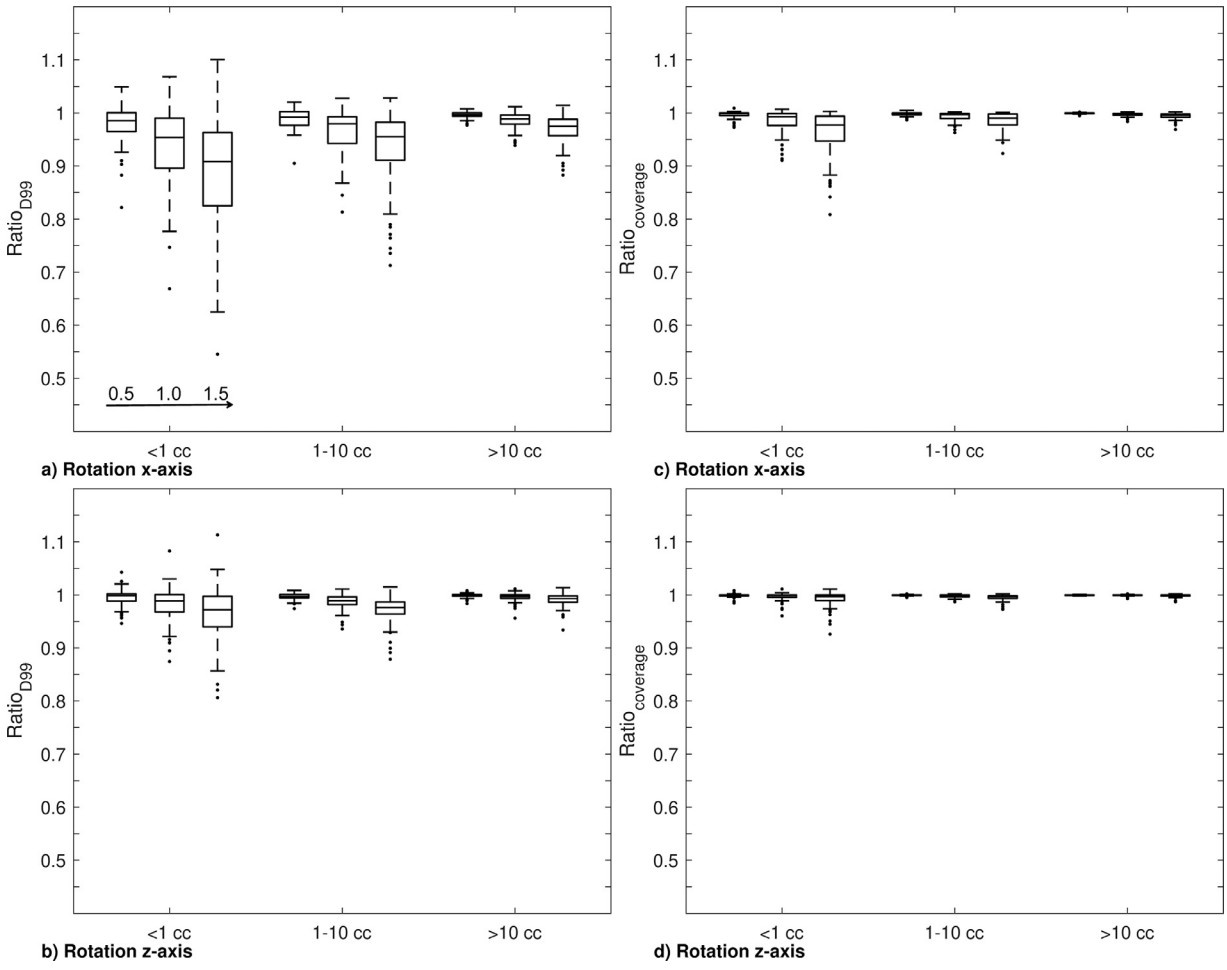

Figure 4 Boxplots of ratio$_{D99}$ (left) and ratio$_{coverage}$ (right) per volume category subdivided in rotation displacements around x-axis **(a, c)** and z-axis **(b, d)**. Per volume category displacement increased from 0.5 mm to 1.5 mm from left-to-right.

significant coefficients of Equations 1 and 2 are listed in Tables 2 and 3, all coefficients are in Table E2. The changes in ratio$_{D99}$ and ratio$_{coverage}$ caused by translations were significantly larger than those caused by rotations ($P < .01$), and keeping the nose-marker displacement constant. For translations the displacement of the targets is equal to the displacement of the nose marker. For rotations around the z-axis, all targets displaced less than the nose marker, and for rotation around the x-axis 18.8% of the targets displaced more than the nose marker. For the mixed-effect model, the mean volume was 12.6 cc, and the mean distance for the rotation was 7.6 cm, and 4.2 cm for the x- and z-axis, respectively.

Table 2 The statistical significant coefficients belonging to the mixed effect model for ratio$_{D99}$ and ratio$_{coverage}$ for translation, Equation 1*

	Ratio$_{D99}$		Ratio$_{coverage}$	
Displ [mm]	α_1	α_2	α_1	α_2
0.5	$-2.2e^{-2}$	$6.4e^{-4}$	$-4.3e^{-3}$	$1.3e^{-4}$
1.0	$-7.1e^{-2}$	$1.9e^{-3}$	$-1.8e^{-2}$	$5.8e^{-4}$
1.5	$-1.3e^{-1}$	$3.1e^{-3}$	$-4.4e^{-2}$	$1.4e^{-3}$

* The intercept equaled 1 in the equations.

The mixed-effect model for translations shows that ratio$_{D99}$ changes by −2.2 %, −7.1%, and −13.0% and ratio$_{coverage}$ by −0.4%, −1.8%, and −4.4% for the mean volume, for a translational displacement of the nose marker of 0.5, 1.0, or 1.5 mm, respectively. Figure 5A illustrates how the ratio$_{D99}$ and ratio$_{coverage}$ change for different volumes and translational displacements. The displacement in the model concerned a factor variable instead of a continuous variable, resulting in a fitted line for each displacement.

For rotational nose-marker displacements of 0.5 mm, 1.0 mm, and 1.5 mm around the x-axis, ratio$_{D99}$ changed by −1.0%, −3.6%, and −6.9%, and ratio$_{coverage}$ by −0.2%, −0.8%, and −1.9%, respectively. For rotational displacement around the z-axis, ratio$_{D99}$ changed by −0.3%, −1.2%, and −2.5%, and ratio$_{coverage}$ by −0.1%, −0.2%, and −0.5%, respectively.

Table 3 The statistical significant coefficients belonging to the mixed effect model for $ratio_{D99}$ and $ratio_{coverage}$ for rotation, Equation 2*

	$Ratio_{D99}$ rotation x-axis				$Ratio_{coverage}$ rotation x-axis			
Displ [mm]	β_1	β_3	β_5	β_6	β_1	β_3	β_5	β_6
0.5	$-1.0e^{-2}$	$3.3e^{-4}$	$-1.7e^{-3}$	$5.5e^{-5}$	$-1.9e^{-3}$	$5.8e^{-5}$	$-3.0e^{-4}$	$9.3e^{-6}$
1.0	$-3.6e^{-2}$	$1.1e^{-3}$	$-5.7e^{-3}$	$1.8e^{-4}$	$-8.0e^{-3}$	$2.6e^{-4}$	$-1.4e^{-3}$	$5.2e^{-5}$
1.5	$-6.9e^{-2}$	$1.9e^{-3}$	$-9.8e^{-3}$	$2.7e^{-4}$	$-1.9e^{-2}$	$6.4e^{-4}$	$-3.5e^{-3}$	$1.4e^{-4}$
Displ [mm]	$Ratio_{D99}$ rotation z-axis				$Ratio_{coverage}$ rotation z-axis			
0.5	$-3.3e^{-3}$	$1.1e^{-4}$	$-1.1e^{-3}$	$4.9e^{-5}$	$-5.9e^{-4}$	$1.8e^{-5}$	$-1.6e^{-4}$	$8.7e^{-6}$
1.0	$-1.2e^{-2}$	$3.8e^{-4}$	$-3.9e^{-3}$	$1.6e^{-4}$	$-2.2e^{-3}$	$7.1e^{-5}$	$-6.4e^{-4}$	$3.0e^{-5}$
1.5	$-2.5e^{-2}$	$7.7e^{-4}$	$-7.7e^{-3}$	$3.1e^{-4}$	$-4.9e^{-3}$	$1.6e^{-4}$	$-1.6e^{-3}$	$7.3e^{-5}$

* The intercept equaled 1 in the equations.

Figure 5B-E depicts how the $ratio_{D99}$ and $ratio_{coverage}$ change as a function of target volume and distances of midpoint-target to rotation axis for rotational displacements. For each displacement, the outcome parameter resulting from the 2 continuous variables (ie, volume and distance midpoint-target to rotation axis) are presented as iso-effect lines (Fig 5).

The conditional R-squared (ie, the proportion of variance explained by the complete model) for the translational displacement model was 0.84 for $ratio_{D99}$, and 0.70 for $ratio_{coverage}$. The conditional R-squared for rotational displacement around the x-axis was 0.74, and for the z-axis 0.78 for $ratio_{D99}$, the R-squared was 0.67 for both x-axis and z-axis for $ratio_{coverage}$. The models show that the change for $ratio_{D99}$ is larger than for $ratio_{coverage}$, and for rotations around the x-axis (nodding) the change was larger than for rotations around the z-axis (looking left-right).

Discussion

We have simulated translations and rotations of targets in actual patient SRS treatment plans to study the effect of predefined nose-marker displacements on dose to the target volume. During a GK treatment with mask immobilization, a threshold is set for the allowed nose-marker displacement. Thus, the simulated displacements could be viewed as used thresholds during treatment. We have determined that increasing this threshold from 0.5 mm to 1.0 mm or 1.5 mm has a significant effect on the dose to the target, D_{99}, and coverage. The effect caused by translational displacement was significantly larger compared with rotational displacements.

The effect on D_{99} and coverage decreases for increasing volumes. This is caused by the fact that small lesions, in this work defined as <1 cc, have a radius of approximately 0.6 mm which can, therefore, move entirely outside the prescribed isodose line given the simulated displacements of 0.5 mm, 1.0 mm, and 1.5 mm. For larger lesions, a smaller percentage of the lesion will displace outside the prescribed isodose line.

For translations, the displacements in z-direction have a larger dosimetric effect than displacements in x- or y-direction. This can, in part, be explained by the fact that the dose gradient in GKI is steeper in z-direction and is thus more susceptible to smaller displacements. The increased dose drop-off in z-direction is caused by the directionality and positioning of the 192 sources. The GKI is based on an arrangement of sources analogous to a band around the head with each source beam focused on a single isocenter, with no beams entering the top and bottom parts of the skull. For other technologies such as linear-accelerator-based SRS, the effect of displacement axis on dosimetric properties will depend on the used beam arrangement and may differ somewhat from the trends observed in the present study.

For rotational displacements, the rotation around the x-axis (ie, nodding motion) had a larger effect on the dose than a rotation around the z-axis (ie, looking left-right). This difference is explained by the distance of the targets to rotation axis, as discussed by Roper et al.[19] In motion traces of the nose marker measured during actual treatments, it has been shown that the z-directional component is always present in the traces[8]; corresponding to rotations around the x-axis and/or a translation effect. The effect on the dose is reduced if this motion is caused by rotation compared with translation. Therefore, it would be highly beneficial to know if the motion of the nose marker is caused by rotation or translation during treatment. Combined with the effect of steeper dose gradients in the z-direction, this information could potentially lead to usage of an anisotropic threshold at the detriment of user friendliness. However, based on the current technology implemented on the system, it is not possible to distinguish between rotation and translation.

The larger effect on the dose of translation compared with rotation can be explained by the fact that for translation, the tumor motion is equal to the nose marker

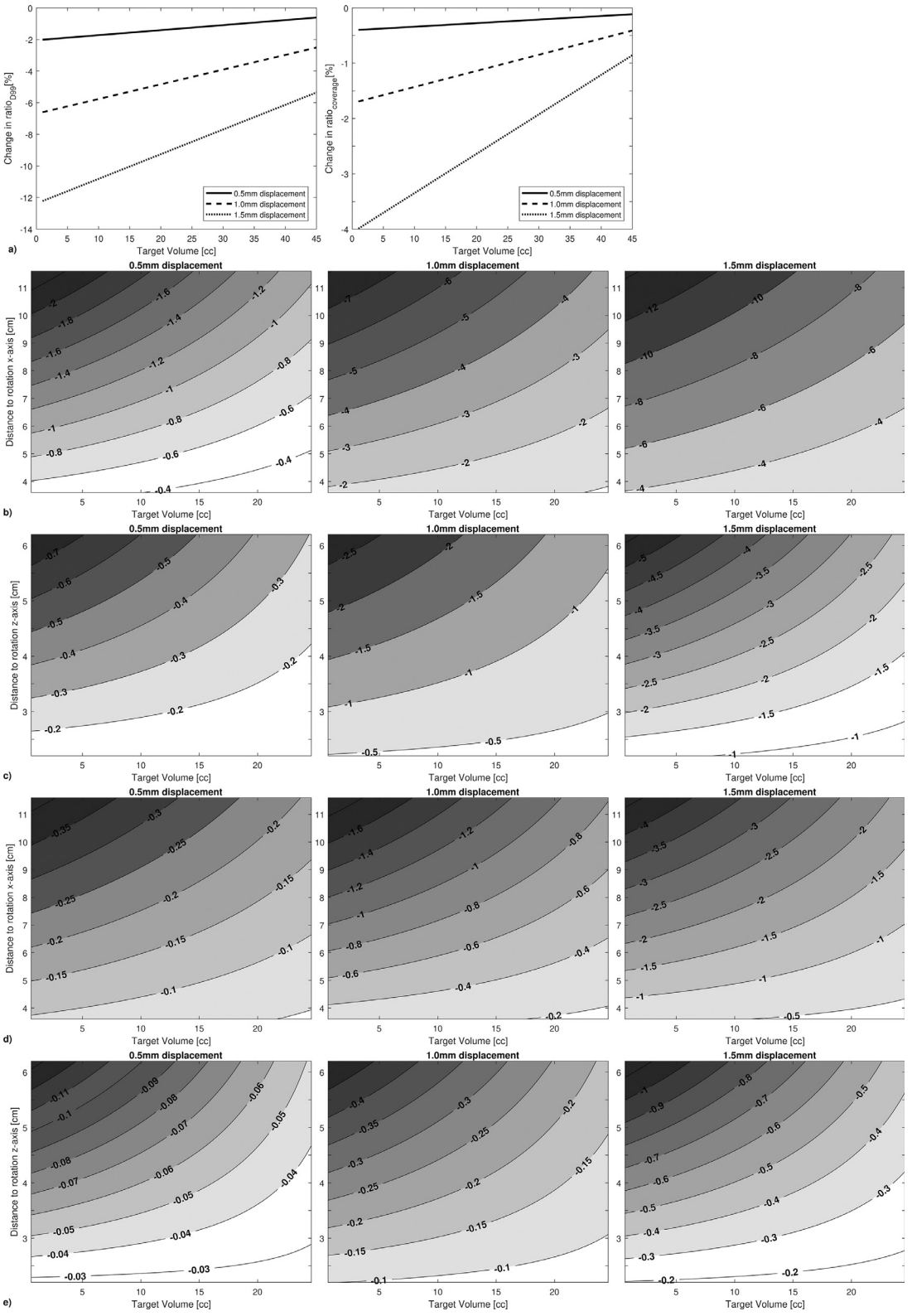

Figure 5 The mixed effect model for **(a)** translation and **(b-e)** rotation displacements. For translation a line per displacement shows the effect on ratio$_{D99}$ (left) and ratio$_{coverage}$ (right) for different volumes. For rotations a plot is made for different volumes and distances midpoint-target to rotation axis, with the iso-effect lines showing the change in ratio$_{D99}$ for rotation around the x-axis **(b)** and z-axis **(c)**, and the change in ratio$_{coverage}$ for rotation around the x-axis **(d)** and z-axis **(e)**.

motion, whereas for rotation around the x-axis 80% of the tumors shifted less than the nose marker; for the z-axis all targets shifted less. Wright et al have shown[6] similar ratios between displacement of the target compared with nose marker, based on intrafraction CBCT information from 22 actual treatments, and also they have determined that intracranial displacements could exceed the nose-marker displacements. Moreover, our study shows that not only the position of the target should be considered when setting the threshold, but also the target volume should be considered.

This work has a few limitations that need to be addressed. First, tumor volumes in the present study were reconstructed in MATLAB by generating a triangulated surface, which may have yielded less accurate volume reconstructions for complex-shaped targets. In addition, MRI slice thickness was larger than the 0.5 mm spatial distance of the dose distribution data. Therefore, interpolation of target contours between MRI slices was necessary. Although we excluded cases in which the reconstruction differed by >10% volume difference, or >2.5% D_{99} difference compared with LGP, we may have introduced a bias in the analysis. Another limitation is that after the displacement the orientation of the head relative to the beams is changed. Based on the small displacements this effect was considered negligible and no adjustment of corresponding attenuations was performed. Another limitation is the method for rotation simulation. In the present study, skull rotation was simplified by (1) using the lowest point of the skull (clivus) as rotation point, (2) defining the rotation axes based on anatomic landmarks, and (3) the assumption that the nose marker moves rigidly with the patients' heads. Although this approach is chosen for its reproducibility across patients, (1) the rotation axes during the actual treatment are unknown and can be located in different locations than those used in the simulations, (2) movement of the patients' heads during treatment while restricted by the mask and cushion is difficult to predict, and (3) in reality the nose can move independently of the head. In addition, a given nose-marker displacement may result from any combination of pure translations and rotations, whereas we evaluated each separately. Another limitation of the present study is that the simulated displacements are taken for the complete duration of treatment, whereas the motion trace of the nose marker can fluctuate during treatment,[8,20] and displacements can be corrected by acquiring an intrafraction CBCT, suggesting that these findings are a worst-case scenario. Another limitation of this study is the implementation of the mixed-effect model. Ideally, the displacement would be considered a continuous variable resulting in a single model for different displacements. Furthermore, the model would improve if more targets had been included. Finally, the data all came from a single GK center. Results may, therefore, be biased because these are based on planning, dose-description, and GKI motion monitoring protocol of that center. For example, results were obtained based on targets treated without PTV margins and 100% coverage. With the use of a threshold, displacement of the tumor during treatment is limited to prevent underdosing. By using PTV margins, an increased displacement of the target may be acceptable, at a cost of irradiating a limited extra amount of normal tissue. In addition, a treatment plan and corresponding dosimetry, also depends on tumor type, shape, and on organs at risk (OAR). The effect of undertreatment of a small part of the target, the effect of an OAR on dosimetry, and the effect of displacement on the dose that an OAR receives was out of the scope of this study. Whether these factors should be considered when setting the threshold has not been evaluated.

More information concerning actual movements of the patient during treatment is needed to validate the simulation model. This validation is part of a future study in a collaboration between multiple Gamma Knife Centers. Despite these limitations, the major strength of the present work has been the development of a systematic and reproducible workflow capable of developing a deeper understanding and modeling of how tumor DVH statistics are affected by known displacements in motion-tracked SRS of a surrogate nose marker.

Conclusions

In this study a quantitative relation between intracranial tumor motion and dosimetric effect is established that can be used to guide decision for appropriate thresholds. Displacement simulations of targets in GKI treatments show that the sensitivity of tumor motion to the dose highly depends on volume and position of the target. This suggests that a patient and target-dependent threshold can be implemented to find an optimal balance between dosimetric plan accuracy and treatment prolongation due to extra CBCTs associated with out-of-tolerance motion. We have shown that this threshold should depend on both location and volume of the tumor, but other factors might need to be included like type of tumor and proximity of an OAR.

Acknowledgments

The authors thank Anton Olsson-Collentine from the Department of Methodology and Statistics at Tilburg University for his statistical support.

Supplementary materials

Supplementary material associated with this article can be found in the online version at https://doi.org/10.1016/j.prro.2021.11.012.

References

1. Leksell L. Stereotactic radiosurgery. *J Neurol Neurosurg Psychiatry*. 1983;46:797-803.
2. Ramakrishna N, Rosca F, Friesen S, Tezcanli E, Zygmanszki P, Hacker F. A clinical comparison of patient setup and intra-fraction motion using frame-based radiosurgery versus a frameless image-guided radiosurgery system for intracranial lesions. *Radiother Oncol*. 2010;95:109-115.
3. Vulpe H, Save AV, Xu Y, et al. Frameless stereotactic radiosurgery on the gamma knife icon: Early experience from 100 patients. *Neurosurgery*. 2020;86:509-516.
4. Babic S, Lee Y, Ruschin M, et al. To frame or not to frame? Cone-beam CT-based analysis of head immobilization devices specific to linac-based stereotactic radiosurgery and radiotherapy. *J Appl Clin Med Phys*. 2018;19:111-120.
5. Guckenberger M, Roesch J, Baier K, Sweeney RA, Flentje M. *Dosimetric consequences of translational and rotational errors in frameless image-guided radiosurgery*. 2012;7:63.
6. Wright G, Schasfoort J, Harrold N, Hatfield P, Bownes P, Phil M. Intra-fraction motion gating during frameless Gamma Knife ® icon^{TM} therapy: The relationship between cone beam CT assessed intracranial anatomy displacement and infrared-tracked nose marker displacement. *J Radiosurg SBRT*. 2019;6:67-76.
7. Kim JO, Fallon K, Bednarz G, et al. Patient motion analysis of first 50 frameless fixation cases with Leksell Gamma Knife ICON. *Int J Radiat Oncol Biol Phys*. 2018;102:e495-e496.
8. MacDonald RL, Lee Y, Schasfoort J, Soliman H, Sahgal A. Ruschin M. Real-time infrared motion tracking analysis for patients treated with gated frameless image guided stereotactic radiosurgery. *Int J Radiat Oncol Biol Phys*. 2020;106:413-421.
9. Ruschin M, Komljenovic PT, Ansell S, et al. Cone beam computed tomography image guidance system for a dedicated intracranial radiosurgery treatment unit. *Int J Radiat Oncol Biol Phys*. 2013;85:243-250.
10. Elekta Instrument AB. *Position accuracy analysis of the stereotactic reference defined by the CBCT on Leksell Gamma Knife ® Icon^{TM}*. Stockholm, Sweden: White Paper; 2015.
11. Elekta Instrument AB. *Geometric Quality Assurance for Leksell Gamma Knife ® Icon^{TM}*. Stockholm, Sweden: White Paper; 2015.
12. Chung HT, Kim JH, Kim JW, et al. Assessment of image co-registration accuracy for frameless Gamma Knife surgery. *PLoS ONE*. 2018;13.
13. Stieler F, Wenz F, Abo-Madyan YM, et al. Adaptierte fraktionierte stereotaktische Strahlentherapie mit dem Gamma Knife bei Meningeom mit cone-beam-CT und adaptiver Replanung (a-gkFSRT). *Strahlentherapie und Onkologie*. 2016;192:815-819.
14. Elekta Instrument AB. *Accuracy of co-registration of planning images with cone beam CT images*. Stockholm, Sweden: White Paper; 2015.
15. AlDahlawi I, Prasad D, Podgorsak MB. Quality assurance tests for the Gamma Knife Icon^{TM} image guidance system. *J Appl Clin Med Phys*. 2018;19:573-579.
16. Nassim Khaled. Straight line and plane intersection. Available at: https://www.mathworks.com/matlabcentral/fileexchange/17751-straight-line-and-plane-intersection, MATLAB Central File Exchange. Accessed February 28, 2021.
17. Matt J. *3D rotation about shifted axis*. 2021. Available at; https://www.mathworks.com/matlabcentral/fileexchange/30864-3d-rotation-about-shifted-axis. MATLAB Central File Exchange. Accessed February 28.
18. Nakagawa S, Johnson PCD, Schielzeth H. A general and simple method for obtaining R2 from generalized linear mixed-effects models. *Methods in Ecology and Evolution*. 2013;4:133-142.
19. Roper J, Chanyavanich V, Betzel G, Switchenko J, Dhabaan A. Single-isocenter multiple-target stereotactic radiosurgery: Risk of compromised coverage. *Int J Radiat Oncol Biol Phys*. 2015;93:540-546.
20. AAPM Radiation Therapy Committee. Task Group 42. Stereotactic Radiosurgery. Published for the American Association of Physicists in Medicine by the American Institute of Physics; 1995.